Cheng Li
Qi Weijun

ISSN 1333-1124
eISSN 1849-1391

ROTATING STALL REGION OF WATER-JET PUMP

UDC 621.22

Summary

There is a rotating stall region, which is the so-called unstable head curve when water-jet is operated. This region should be usually avoided because of the risk of instabilities during the pump starting and operation. Experimental and numerical research on the relation between the instability in the head curve and the magnitude of unsteady hydraulic forces are presented. It is found that the rotating stall region is strongly influenced by the clearance gap between the impeller blades and the casing. The head increases over the entire range of flow rates when the tip clearance is reduced. The spectral content of the forces shows evidence of rotating instabilities. It is indicated that the instability of the head curve and unsteady forces are interrelated, and that rotating instabilities play a role in this unstable operation region.

Key words: *water-jet pump, unstable, rotating stall, numerical simulation*

1. Introduction

It has become clear that there is a relationship between the magnitude of blade interaction forces and the shape of the head characteristic of the water-jet pump, notably in the region of rotating stall. Moreover, the size of the tip-clearance of the semi-open mixed flow impeller has shown to have an influence on the instability of the head curve. This was the motivation to study the relation between the head instability, the occurrence of unsteady forces, and the influence of tip clearance.

The decrease in the magnitude of forces on the impeller and shaft system of pumps is an important issue during the design of a pump as well as during the pump operation. It is well known, for instance, that volute pumps can have large steady radial loading on the shaft when operated at off-design conditions. That is why, for example, boiler feed pumps exhibit a vanned diffuser casing to reduce the steady load. Research in the past has revealed that, although the steady load is reduced considerably, the unsteady forces tend to be higher compared to a similar pump equipped with a volute. Over the last few decades, extensive research has been done to asses the origin and magnitude of these forces. Forces are especially strong in high head pumps. For this reason, most of the research in the past has been concentrated on centrifugal pumps of radial type. However, pumps of low and intermediate head, like axial and mixed-flow pumps, can also be subjected to forces of

considerable magnitude. One of the examples is water-jet pumps [1], often of mixed-flow type, used to propel ships. These pumps can operate at high speeds, yet free of cavitation, due to the high suction pressure available. Forces on the impeller, both steady and unsteady, are strong and can cause wear, fatigue failure and vibrations up to a level that makes travelling aboard these ships an uncomfortable experience. On the other hand, hydrodynamic excitation forces result from a variety of unsteady flow phenomena such as stall, flow recirculation, cavitation, and blade interaction, whereas hydrodynamic reaction forces may result from the rotor whirl or processing motion relative to the casing[2-4] .

Rotating stall is well-known from compressor practice. It was explained first by Emmons et al. [5]. Rotating stall appears also on pump blades [6].The shape of the pump characteristics may give some information about the development of the stall (Fig. 1). If a mixed-flow or an axial-flow pump is tested at a constant speed with gradually increasing head, the blades operate with increasingly greater incidence angle, and, at a certain angle, stall inception takes place. In standard designs, the first signs of stall appear on the blade sections near the hub. The local head produced by these stalling blade sections brakes down (like the lift coefficient of the air foils). Thus, the contribution of the stalling sections to the head is missing,. Therefore, (i) the head characteristics gradually depart from their general trends (Fig. 1), and (ii) a backflow occurs at the hub (Fig. 3). This secondary flow is also a consequence of stall. The rotating stall region affected the safety of pump start-up and limited the range of stable operating [7-10]. When there are three flow rate points matching one lift, the hydraulic unstable operating region occurs. The range region of unstable operation region was from the peak to the bottom of performance curve when the axial flow pump was tested on the closed test rig.

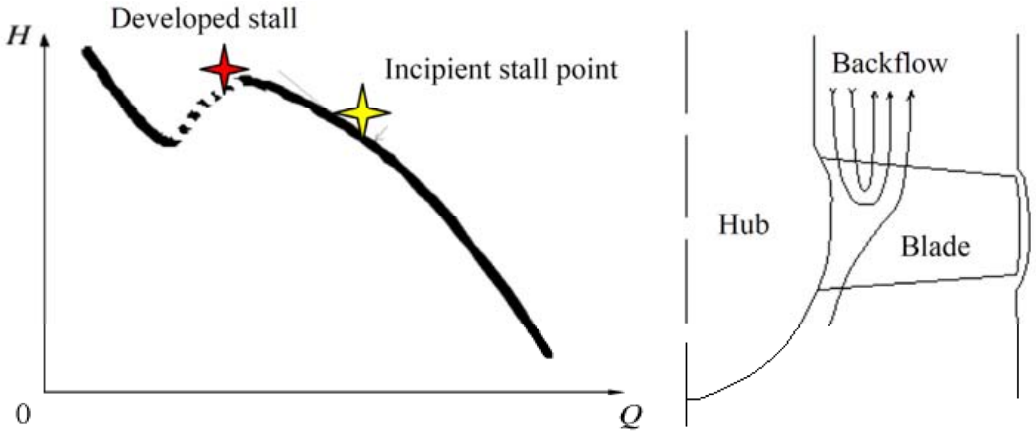

Fig. 1 Stall of pump and backflow

This paper shows that there is a strong influence of the clearance between the impeller blades and the casing. The head increases over the entire range of flow rates when the tip clearance is reduced. The spectral content of the forces shows evidence of rotating instabilities.

2. Experiments

A test facility is built which consists of a closed-loop circuit with a total length of 18 m and a pipe diameter of 315 mm (Fig. 2). Static pressure is measured upstream and downstream of the pump at four pressure taps along the circumference of the pipes. A force

sensing device is placed between the impeller and the shaft so as to directly measure the forces acting on the impeller. The tip clearance is defined as s, the gap between the tip of blade and the casing (Fig. 3). Signals from pressure transducers, along with the signals of six bridges and an optical encoder, are sampled during approximately 500 shaft revolutions and are ensemble (or phase-) averaged. Additional runs with a disc of different weight at different positions revealed that the weight and the axial location of its centre of mass can be determined with an accuracy of 0.1 and 0.2 percent, respectively. The error in the phase angle was less than 1.5 degree. The error in instantaneous forces, determined from the standard deviation in the ensemble averaged signal, was 3 percent. The total error in hydraulic performance was less than 2.5%.

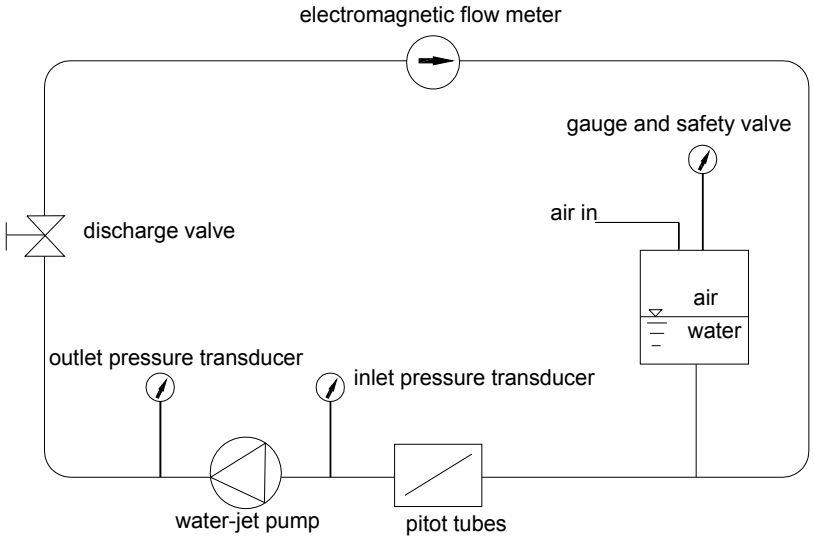

Fig. 2 Experimental facility

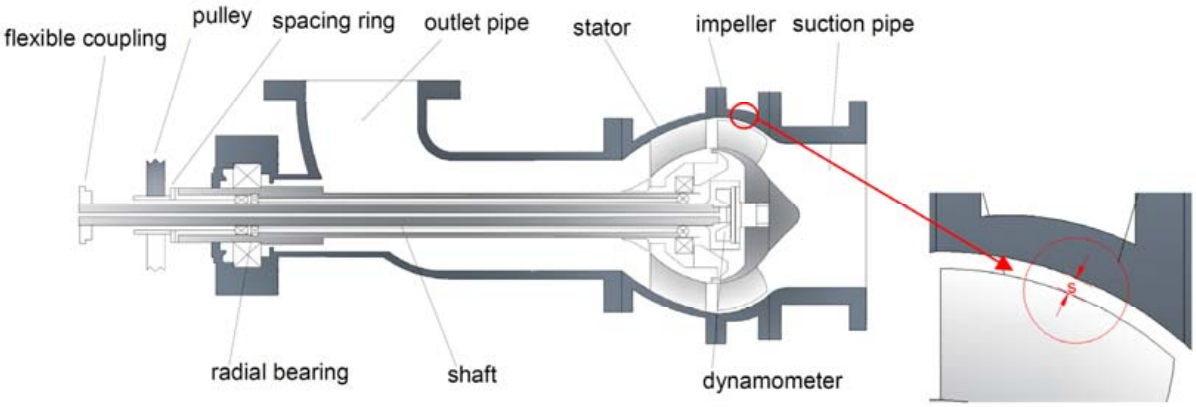

Fig. 3 Cross section of the mixed-flow pump

3. Numerical Simulations

Calculations are performed using the commercial code FLUENT®. The numerical model is based on the Reynolds-Averaged Navier-Stokes (RANS) equations with the standard k-ε model to calculate the Reynolds stresses. First-order upwind discretizations are used for the convective terms and turbulent kinetic energy and dissipation, while the second-order central differencing scheme is used for the diffusive terms. The temporal discretization is second-order implicit. The SIMPLE algorithm is used for the pressure-velocity coupling.

The numerical domain consists of the inlet and outlet passages, the mixed flow impeller with six blades and the diffuser with seven vanes. Inflow and outflow boundaries are located sufficiently far away from the pump not to influence the flow characteristics. Using an extrusion method, an O-type grid of hexagonal cells is created around the impeller and stator blades to ensure good mesh quality in terms of size and skewness. Because of the complex topology of the pump, the interior of the domain is filled with an unstructured mesh of tetrahedral cells (Fig. 4). The inlet boundary condition is specified as a uniform velocity, whereas an outflow boundary condition is applied at the outlet, which allows for non-uniformity in both velocity and pressure. No-slip boundary conditions and wall functions are used for the solid walls.

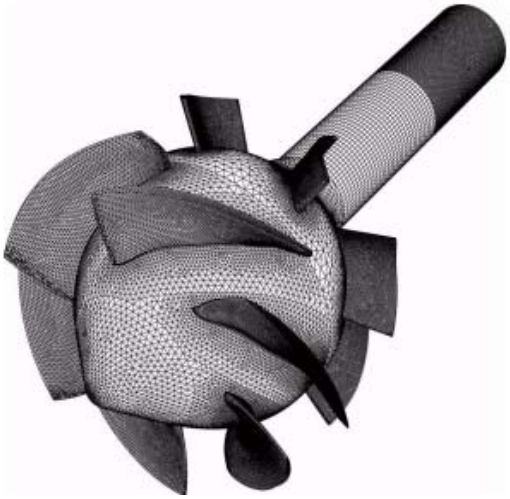

Fig. 4 Surface mesh of rotor and stator

4. Results

Experiments are performed for different shaft speeds ranging from 700 to 900 rpm. Reynolds numbers are in the range $8\sim11\times10^6$ based on the Best Efficiency Point (BEP) operation. Flow rates are varied between 10% and 120% of Q_{BEP}. Measurements are done at different clearances between the impeller blade tip and the casing: a normal value of 0.45 mm (0.15% D_1) and two larger clearances of 0.75 mm (0.25% D_1) and 1 mm (0.33 % D_1). By adjusting the thickness of the spacing ring, the impeller is effectively positioned somewhat closer to the stator vanes. All CFD calculations are done for a shaft speed of 700 rpm and roughly in the same range of flow rates. The impeller tip clearance s is 1 mm.

4.1 Head performance characteristics

Fig. 5 presents head characteristic curves at different shaft speeds and tip clearances. The manometric head was determined from the measured static pressure difference and averaged axial velocity. Results for different shaft speeds are scaled according to similarity theory. The curves show an unstable operating range at part-load conditions, which is typical of pumps of mixed-flow and of axial flow type. In practice, this could lead to unstable operation depending on the system properties and the operating conditions.

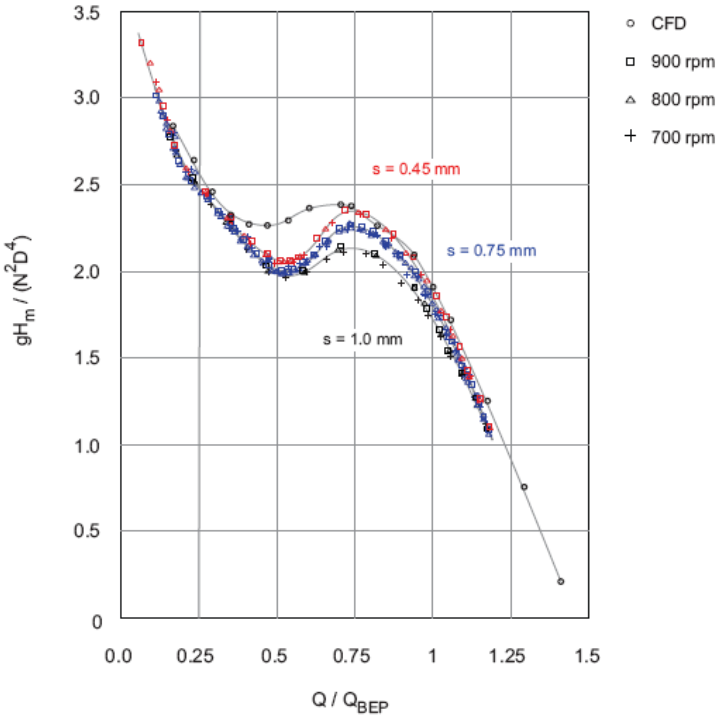

Fig. 5 Manometric head for different shaft speeds and tip clearances
(CFD calculations with s = 1mm)

Results are presented for various tip clearances of the impeller blades. It turns out that the head increases across the entire range of flow rates when the tip clearance is reduced. While this is a common phenomenon observed in all centrifugal pumps with (semi-) open impellers, it also shows that the positive slope of the head characteristic increases with the decreasing tip clearance.

Unsteady CFD calculations tend to overpredict the measured head values, but are in good qualitative agreement. Only in the unstable operating range of the curve, between 45% and 75% Q_{BEP}, a large deviation is observed. For flow rates below 40% Q_{BEP}, the local backflow regions at the impeller inlet near the shroud and at the impeller exit near the hub are well predicted. As a result, the incidence angles along the leading edges of the blades are restored to a more favourable value, thus preventing stalling of the blades. Results for the head at low flow rates in Fig. 4 show that this effect is captured well in the CFD calculations.

4.2 Blade interaction forces

From the bridge signals, one can calculate the instantaneous radial force and bending moment on the impeller. They show spectral content with main contributions at frequencies equal to the shaft frequency and higher harmonics. Among these higher frequencies, the 7th harmonic is dominant. Since this is the frequency of blade passage in the rotating frame of reference, the force is assumed to result from the interaction between the impeller blades and the diffuser vanes. Hence, these unsteady forces are designated ‘blade interaction forces’. They are defined as F_{bb} , the root square value of x and y direction forces.

Results of blade interaction forces, as measured in the pump with a shaft system, are shown in Fig. 6 for different flow rates. Only when the forces are analysed based on the

dynamic calibration of the system do the forces roughly scale with the shaft speed squared, as can be seen from Fig. 7. The measurements of blade interaction forces are given in Fig. 7. Scaling of the forces with the shaft speed is excellent.

The dependency of the force on the flow rate is different from what is normally expected in this type of pump, viz. blade interaction forces increasing at off-design conditions. In this particular pump, the measured forces show a changing magnitude with clear minima around 35% and 70% Q_{BEP}, and maxima around 55% and 95% Q_{BEP}. To the knowledge of the authors, only one group has reported similar results in the past. Kanki (1981) found that one of the pumps considered showed local minima in forces at the blade passing frequency for flow rates of 30% and 70% Q_{BEP}. The pump was of radial end-suction type, with 6 impeller blades and 12 stator vanes. Kawata (1984) found local minima at 50% and 75% Q_{BEP} for a similar pump with 5 impeller blades and 9 stator vanes, but only under severely cavitating conditions. When operating without cavitation, the force at the blade passing frequency showed a single minimum at the BEP condition.

For the unsteady CFD calculations, the hydraulic force on the impeller is determined by the integration of the pressure and shear forces on all rotating surfaces of the pump. This was done for several time steps during one stator pitch passage. The magnitude of the resulting blade interaction force is also given in Fig. 6. The calculated result shows good qualitative agreement with the measurements. The local minimum at 35% Q_{BEP} and the maximum at 95% Q_{BEP} are predicted well. The local maximum at 55% and minimum at 70% Q_{BEP} are not captured. This can be explained by referring to Fig. 6 from which it can be concluded that the onset of stall at the impeller blades is not predicted well. It seems that the flow characteristics in the range 45-75% Q_{BEP} are different from what is calculated numerically.

In Fig. 6, results of blade interaction forces are presented for two different values of the tip clearance. Apparently, blade interaction forces increase if the tip clearance is reduced. This is rather unexpected because a reduction in the tip-clearance size in this particular pump was obtained by increasing the gap between the impeller and the diffuser. One would expect the blade interaction forces to decrease as a result.

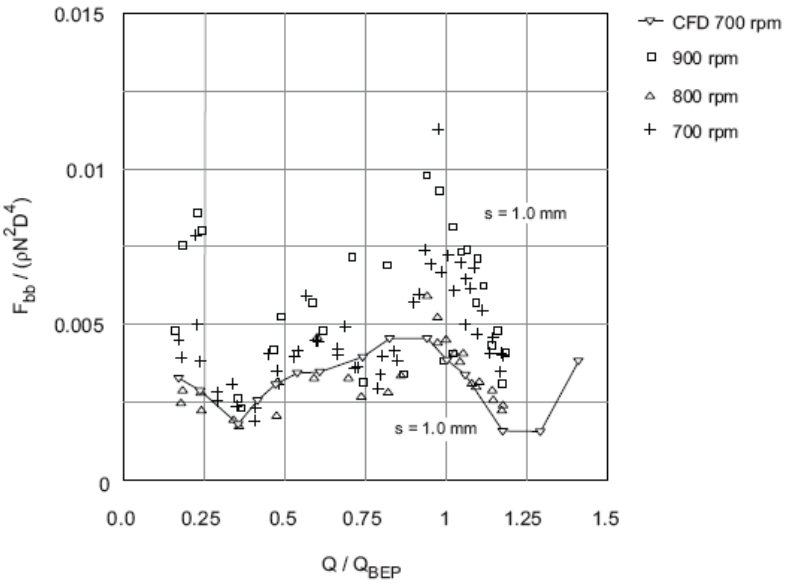

Fig. 6 Blade interaction forces F_{bb} for the same tip clearance compared with CFD results

If the change in the blade interaction forces with the flow rate is compared to the shape of the head characteristic, one observes a correlation between the two. One of the two minima of the blade interaction forces, at 70% Q_{BEP}, coincides with the local maximum of the head curve in the unstable operating region. The local minimum of the head curve in the unstable region in turn coincides with the local maximum of the blade interaction forces, at 55% Q_{BEP}. This combined with the finding that the extent of the instability in the head curve and the blade interaction forces both increase with decreasing tip clearance, leads to the conclusion that the head curve instability and the variation in blade interaction forces are both observations of a common phenomenon.

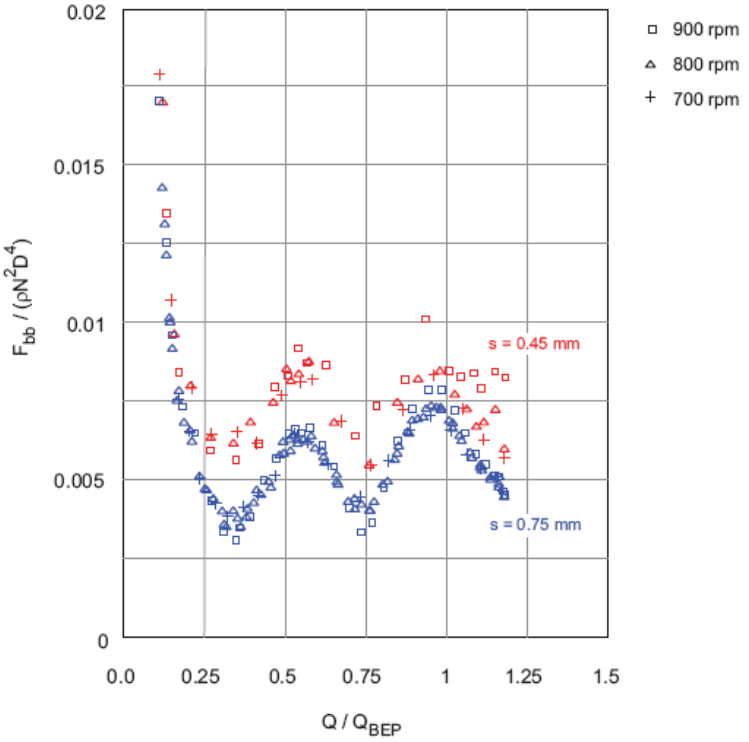

Fig. 7 Blade interaction forces F_{bb} for two different blade tip clearances

4.3 Rotating stall

Fig. 8(a) gives a frequency spectrum of one of the force components in radial direction, as measured in the rotating frame of reference. Results are given for different flow rates, ranging from 10% to 120% Q_{BEP}. The spectra are unfiltered and clearly show the main contributions at shaft frequency N and blade passing frequency ($7N$). An increase in broadband noise at low frequency for flow rates below 70% Q_{BEP} is observed. This is commonly attributed to the occurrence of inlet recirculation, stall or turbulence at a low flow rate.

There are some frequencies in the spectrum at which forces tend to have a higher magnitude than the average. This can be better noted in Fig. 8(b), which shows a narrower range of frequencies. These frequencies seem to shift to slightly lower values as the flow rate is reduced, resulting in a band in the figure that does not seem to have any relation to the shaft speed. The phenomenon can thus be attributed to rotating instabilities, just as the rotating stall.

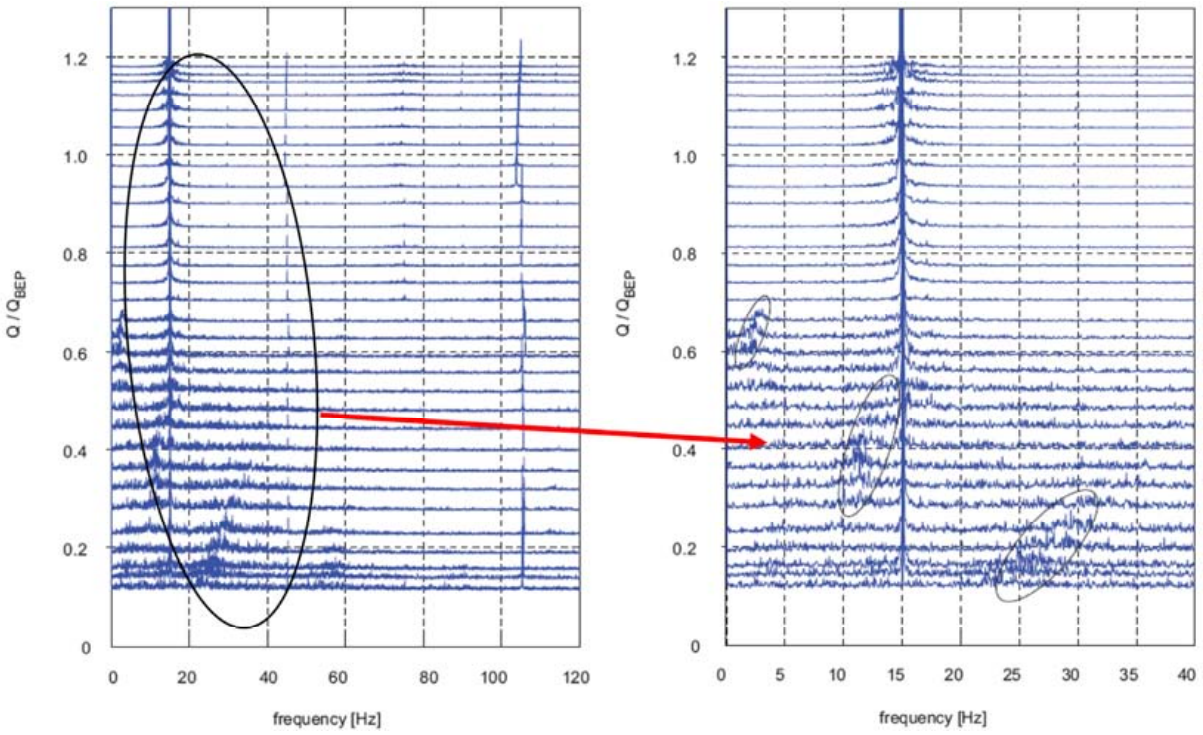

(a) all range of frequency (b) small range in frequency

Fig.8 Spectra of one of the radial force components in the rotating frame of reference at 900 rpm

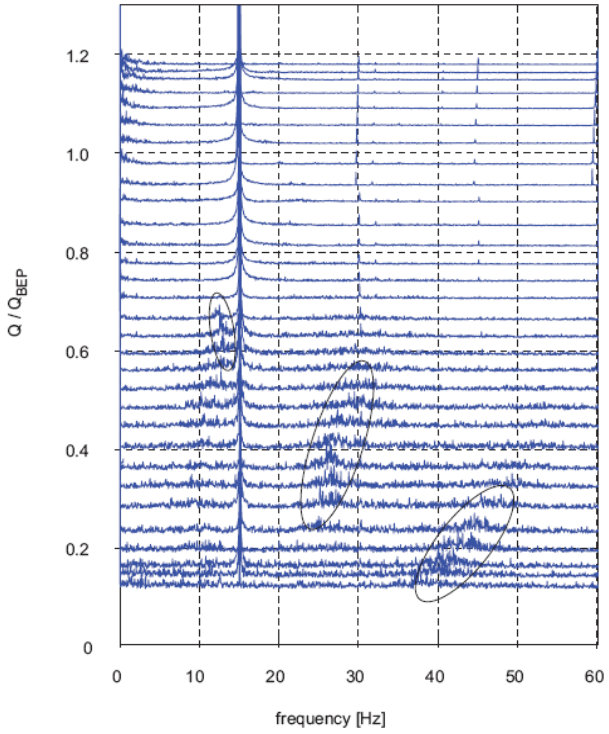

Fig. 9 Spectra of the horizontal component of the radial force in the steady frame of reference at 900 rpm

The radial force on the impeller can be transformed from the rotating frame, in which it was measured, to the steady frame of reference. Fig. 9 shows the spectra of the horizontal component of the radial force in the steady frame of reference. It shows that the rotating stall first occurs at 70% Q_{BEP} at a rotation speed slightly below the shaft speed. The speed of the

instability approaches the shaft speed as the flow rate is reduced further until it reaches the shaft speed at around 50% Q_{BEP}. At 55% Q_{BEP}, the second instability occurs, which rotates at twice the shaft speed. If the flow rate decreases, this instability rotates at ever lower speeds until it disappears at 30% Q_{BEP}. At that point, the third instability takes over, rotating at around three times the shaft speed. Also, this rotational speed decreases when the flow rate is reduced further.

5. Conclusions

This paper focuses on the relationship between the head characteristic of a water-jet pump, the occurrence of unsteady forces and rotating stall. It was found that the main contribution to unsteady forces is made by a frequency equal to the blade passing frequency. The magnitude of the unsteady forces shows a variation with flow rate. In contrast to what was expected, the minimum value was not at the design flow rate. Instead, unsteady forces show clear minima at 30% and 70% Q_{BEP}, and local maxima at 55% and 95% Q_{BEP}. Moreover, the local minimum at 70% and the local maximum at 55% Q_{BEP} happen to coincide with the local maximum and minimum of the head characteristic in the unstable region. This evidence of causality between unsteady forces and unstable head curve is further strengthened by the observation that both the extent of the instability of the head curve and the unsteady force increase with the decreasing value of the clearance between the tip of the impeller blades and the casing.

Results showing the spectral content of radial forces on the impeller give evidence of the existence of instabilities at frequencies not related to the shaft frequency, like for rotating stall. These instabilities emerge at flow rates below 70% Q_{BEP}, at frequencies which vary with the flow rate. When the flow rate is reduced gradually, the frequency of instability suddenly changes from the near shaft frequency to the two times shaft frequency, at 55% Q_{BEP}, and to the three times shaft frequency at around 30% Q_{BEP}. This shows that the character of the unstable flow phenomenon suddenly changes at these flow rates. It is indicated that not only the instability of the head curve and unsteady forces are interrelated, but also that the rotating stall plays a role in this phenomenon. CFD calculations show good qualitative agreement with the measured head characteristic, except for the rotating stall region. The disagreement in this region is probably due to the rotating instability which combines stall phenomena with an inherently unsteady flow.

6. Acknowledgments

This work was financially supported by the National science and technology plan project in rural areas (Grant No.2012BAD08B03), National Natural Science Foundation of China (Grant No. 51179167, 51010105026, 50809057) , the Scientific Research Foundation for the Returned Overseas Chinese Scholars, State Education Ministry(Grant No. 2010(1561)) and Major Natural Science Foundation of Universities in Jiangsu(Grant No.12KJA570001).

REFERENCES

[1] Bulten N W H, Van Esch B P M. *Fully transient cfd analyses of waterjet pumps*, *Marine Technology*, 2007 , 44(3): 185-193

[2] EHRICH F F, CHILDS D W. *Self-excited vibrations in high performance turbomachinery*. *Mechanical Engineering*, 1984,106(5):66-79.

[3] Gülich J, Bud W, Hughes S F. *Review of parameters influencing hydraulic forces on centrifugal impellers*, *Proceedings of Institution of Mechanical Engineers*, 1987, 201(2): 163-174

[4] Ohashi H, Imai H, Tsuchihashi T. *Fluid Force and Moment on Centrifugal Impellers in Precessing Motion*, *ASME Fluid Machinery Forum*, Portland, USA, June 23-27(1991)

[5] Emmons, H.W., Pearson, C.E., and Grant, H.P. *Compressor surge and stall propagation, Trans. ASME 79, 1955*:455-469

[6] Brennen, C.E. *Hydrodynamics of Pumps, Concepts ETI and Oxford University Press,* 1994

[7] Liu Chao,Tang Fangping,Zhou Jiren,et al. *Large vertical axial-flow pump system performance and stability analysis* . China water supply and drainage, 2003(3):69-71

[8] Yuan Jiabo,Tang Fangping,Cheng Li. *Discussion on some problems of axial flow pump operation*. Pump technology, 1999,(5):29-32

[9] Li Shihuang. *At off-design condition and optimum design of vane pump*. Beijing: Machinery Industry Press,2006,1

[10] Luo Shihong,Zhu Huaming,Liu Chaofu,et al. *Large scale X type flow passage of pumping unit vibration technology research* . Drainage and irrigation machinery, 2001, 19 (4): 15-20

Submitted: 30.12.2013

Accepted: 04.6.2014

Prof. Dr. Cheng Li
Mr. Qi Weijun
School of Hydraulic, Energy, and power Engineering, Yangzhou University
Jiangyang Middle Road 131, Yangzhou, Jiangsu, P.R. China